DRAFT VERSION FEBRUARY 8, 2022
Typeset using LaTeX **twocolumn** style in AASTeX631

arXiv:2202.02683v1 [astro-ph.EP] 6 Feb 2022

Fine-grained rim formation via kinetic dust aggregation in shock waves around evaporating icy planetesimals

SOTA ARAKAWA,[1] HIROAKI KANEKO,[2] AND TAISHI NAKAMOTO[2]

[1]*Division of Science, National Astronomical Observatory of Japan, 2-21-1 Osawa, Mitaka, Tokyo, 181-8588, Japan*
[2]*Department of Earth and Planetary Sciences, Tokyo Institute of Technology, 2-12-1 Ookayama, Meguro, Tokyo, 152-8550, Japan*

ABSTRACT

Fine-grained rims (FGRs) are frequently found around chondrules in primitive chondrites. The remarkable feature of FGRs is their submicron-sized and non-porous nature. The typical thickness of FGRs around chondrules is 10–100 μm. Recently, a novel idea was proposed for the origin of FGRs: high-speed collisions between chondrules and fine dust grains called the kinetic dust aggregation process. Experimental studies revealed that (sub)micron-sized ceramic particles can stick to a ceramic substrate in a vacuum when the impact velocity is approximately in the range of 0.1–1 km/s. In this study, we examine the possibility of FGR formation via kinetic dust aggregation in chondrule-forming shock waves. When shock waves are created by undifferentiated icy planetesimals, fine dust grains would be released from the planetary surface due to evaporation of icy planetesimals. We consider the dynamics of chondrules behind the shock front and calculate the growth of FGRs via kinetic dust aggregation based on simple one-dimensional calculations. We found that non-porous FGRs with the thickness of 10–100 μm would be formed in shock waves around evaporating icy planetesimals.

1. INTRODUCTION

Fine-grained rims (FGRs) are frequently found around chondrules and calcium-aluminum-rich inclusions (CAIs) in primitive chondrites. FGRs are distinguishable from the interchondrule matrix in optical and scanning electron microscopy images as they have different texture and composition, and the typical thickness of FGRs is on the order of 10–100 μm (e.g., Matsunami 1984; Hanna & Ketcham 2018). The physical mechanism that produced these rims is still under debate, and several scenarios have been suggested so far (e.g., Metzler et al. 1992; Trigo-Rodriguez et al. 2006; Takayama & Tomeoka 2012; Liffman 2019).

The majority of studies assumed that FGRs were formed via the accretion of dust particles onto the surfaces of chondrules/CAIs in the turbulent solar nebula (e.g., Metzler et al. 1992; Morfill et al. 1998; Cuzzi 2004; Xiang et al. 2019, 2021; Matsumoto et al. 2021; Kaneko et al. 2022). This nebular scenario naturally reproduces the positive correlation between the rim thickness and the chondrule radius, which is reported for FGRs around chondrules in CM chondrites (e.g., Metzler et al. 1992; Hanna & Ketcham 2018; Zanetta et al. 2021).

However, Liffman (2019) pointed out that the nebular scenario has a difficulty explaining the low porosity of FGRs. Assuming that collisions between chondrules and fine grains occurred in the turbulent solar nebula, the impact velocity would be approximately or lower than 1 m/s and porous dust rims with the porosity of approximately 60% would be formed (Beitz et al. 2013a). In addition, dust grains turned into fluffy aggregates prior to the accretion onto chondrules when the grain size is smaller than 1 μm (e.g., Arakawa 2017; Matsumoto et al. 2019; Kaneko et al. 2022). The typical grain size of FGRs in primitive chondrites is indeed submicron (e.g., Lauretta et al. 2000; Chizmadia & Brearley 2008; Zanetta et al. 2021), although grain size might be subsequently modified by aqueous/thermal alteration processes. Hence the structure of FGRs formed in the turbulent solar nebula would be highly porous; which seems to be inconsistent with the observed compact FGRs with low porosity of 10–20% (e.g., Trigo-Rodriguez et al. 2006).

Alternatively, several studies investigated a scenario that FGRs were formed after accretion of chondrite parent bodies (e.g., Sears et al. 1993; Trigo-Rodriguez et al. 2006; Tomeoka & Ohnishi 2010; Takayama & Tomeoka 2012). In the framework of this parent-body scenario, the FGRs are formed via aqueous/thermal alterations of host chondrules and/or via impact-induced compaction/fragmentation of the matrix material around chondrules (see Tomeoka & Ohnishi 2010, and references therein). The parent-body scenario can naturally explain the non-porous nature of FGRs, and this is one of the reasons why parent-body scenario is still favored for the origin of FGRs. However, another difficulty exists when we consider the parent-body scenario. Based on the fabric analysis by high-resolution electron backscatter diffraction, Bland et al. (2011) found that FGRs were exposed to a spherically symmetric stress field while the matrix exhibits a bulk uniaxial stress field. This result indicates that FGRs were compressed prior to rimmed chondrules being incorporated into chondrite parent bodies. Moreover, Beitz et al. (2013b) revealed that impact-induced compaction cannot form non-porous FGRs, based on their impact experiments into mixtures of chondrule analogs and fine dust particles.

To solve these problems, Liffman (2019) proposed a novel idea for the origin of FGRs: high-speed collisions between chondrules and fine dust grains called the *kinetic dust aggregation* process. The kinetic dust aggregation is also known

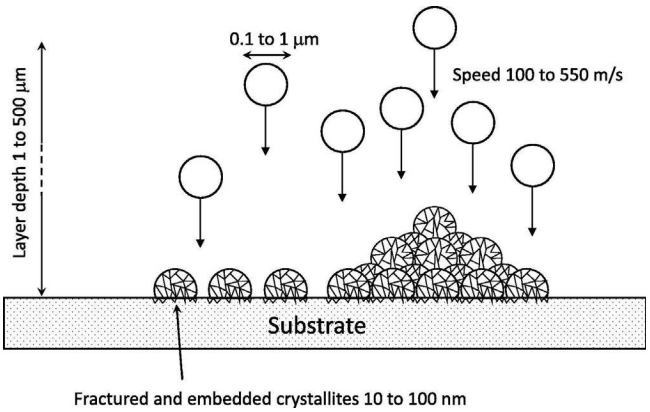


Figure 1. Illustration of the fracturing and compaction of dust particles during kinetic dust aggregation. Note that the maximum/minimum velocities for adhesion shown in this figure (100 and 550 m/s) are for the case of (sub)micron-sized yttrium iron garnet ($Y_3Fe_5O_{12}$) particles, and these critical velocities should depend on the composition and grain size in reality. Figure taken from Liffman (2019) modified after Johnson et al. (2014).

as the aerosol deposition method (e.g., Akedo 2006, 2008; Akedo et al. 2008; Johnson et al. 2014; Hanft et al. 2015) in the field of ceramic coating technologies. Experimental studies revealed that (sub)micron-sized ceramic particles can stick to a ceramic substrate in a vacuum, and the impact velocity for sticking is approximately 0.1–1 km/s (see Hanft et al. 2015, and references therein). Molecular dynamics simulations also confirmed that 10–100 nm-sized brittle nanoparticles can stick to the substrate when the impact velocity is on the order of 0.1–1 km/s (e.g., Daneshian & Assadi 2014). The resulting dust layer formed via the kinetic dust aggregation have low porosity and are fine grained, as illustrated in Figure 1. Therefore, we can reproduce the observed structure of FGRs if they are formed via the kinetic dust aggregation process, which should be related to chondrule-forming supersonic events.

In this study, we examine the possibility of FGR formation via kinetic dust aggregation in chondrule-forming shock waves. Shock waves caused by eccentric planetesimals in the gaseous solar nebula is one of the leading candidates for the chondrule-forming transient events (e.g., Weidenschilling et al. 1998; Ciesla et al. 2004; Morris et al. 2012; Mann et al. 2016; Mai et al. 2018; Nagasawa et al. 2019). When shock waves are created by undifferentiated icy planetesimals, fine dust grains would be released from the planetary surface due to evaporation of icy planetesimals (e.g., Tanaka et al. 2013). The enrichment of fine dust grains in chondrule-forming environment would be preferred from a variety of perspectives (e.g., Alexander et al. 2008; Hewins et al. 2012; Tenner et al. 2015). Based on the oxygen isotope composition and oxidation state of chondrule olivine, Schrader et al. (2013) concluded that chondrules in CR chondrites formed under H_2O/H_2 ratios between 10 and 1000 times the solar ratio (see also Tenner et al. 2015). As evaporating icy planetesimals can supply high H_2O vapor

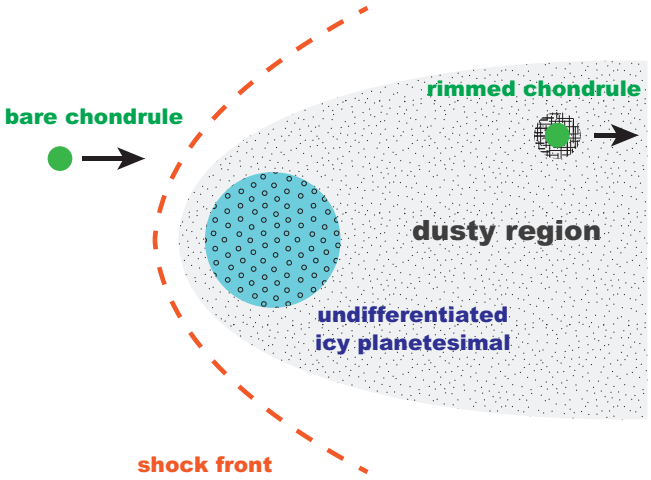


Figure 2. Schematic of our fine-grained rim formation scenario. Evaporation of undifferentiated icy planetesimals produces dusty regions behind the shock front. As chondrules entered the shock wave have a relative velocity with respect to fine grains, which are dynamically coupled with gas, fine dust grains collide with chondrules and fine-grained rim will be formed in dusty regions.

pressure, our scenario is also consistent with the observed oxygen fugacity. We consider the dynamics of chondrules behind the shock front and calculate the growth of FGRs via kinetic dust aggregation. Although our numerical results are based on simple one-dimensional calculations, we found that non-porous FGRs with the thickness of 10–100 μm would be formed in shock waves around evaporating icy planetesimals.

2. MODEL

2.1. *Outline*

The formation process of FGRs in shock waves is illustrated in Figure 2. We consider the accretion of FGRs onto bare chondrules. When shock waves are caused by undifferentiated icy planetesimals, the dusty region would be formed behind the shock front due to evaporation of planetesimals. We assume that fine dust grains released from planetesimals are dynamically coupled with gas while chondrules entered the shock wave have relative velocity with respect to gas, and fine dust grains collide with chondrules. Then fine dust grains accrete onto chondrules if the impact velocity satisfies the condition for adhesion.

We briefly explain the models and settings in the following sections. In this study, we discuss the dynamics of chondrules in one-dimensional normal shocks. The basic framework of our model is identical to that used in Arakawa & Nakamoto (2019). We calculate the evolution of the velocity and radius of rimmed chondrules, v and r, simultaneously.

2.2. *Gas structure*

We do not calculate the dynamics of gas behind the shock front but assume a simple gas structure. Then the dynamics of chondrules is simulated in the given gas flow. We assume

that the gas velocity with respect to the shock front, $v_{\rm g}$, and the gas density, $\rho_{\rm g}$, evolve as functions of the distance from the shock front, x:

$$v_{\rm g} = \begin{cases} v_0 & (x < 0), \\ v_0 + (v_{\rm post} - v_0)\exp\left(-x/L\right) & (x \geq 0), \end{cases} \quad (1)$$

and

$$\rho_{\rm g} = \frac{v_0}{v_{\rm g}}\rho_{\rm g,0}, \quad (2)$$

where v_0 is the pre-shock gas velocity with respect to the shock front, $v_{\rm post}$ is the post-shock gas velocity with respect to the shock front, $\rho_{\rm g,0}$ is the pre-shock gas density, and L is the spatial scale of the shock. The spatial scale of the shock should be several times or much larger than the radius of planetesimals, $r_{\rm p}$ (see Arakawa & Nakamoto 2019, and references therein). However, the value of L should also depend on the physical properties of the solar nebula, e.g., the turbulence strength and the opacity. Thus we regard L as a parameter and consider three cases: $L = 3 \times 10^4$ km, 1×10^4 km, and 3×10^3 km. The post-shock gas velocity, $v_{\rm post}$, is given by $v_{\rm post} = [(\gamma - 1)/(\gamma + 1)]v_0$, where γ is the ratio of specific heats. We set $\rho_{\rm g,0} = 5 \times 10^{-10}$ g cm^{-3}, $v_0 = 12$ km s^{-1}, and $\gamma = 1.4$. Similarly, the temperature of the gas $T_{\rm g}$ is assumed as follows:

$$T_{\rm g} = \begin{cases} T_0 & (x < 0), \\ T_0 + (T_{\rm post} - T_0)\exp\left(-x/L\right) & (x \geq 0). \end{cases} \quad (3)$$

We assume that the pre-shock gas temperature is $T_0 = 200$ K and the post-shock gas temperature is $T_{\rm post} = 1600$ K. The most probable molecular velocity $c_{\rm s}$ is given by $c_{\rm s} \equiv (2k_{\rm B}T_{\rm g}/m_{\rm g})^{1/2} = 1.3\ [T_{\rm g}/(200\ {\rm K})]^{1/2}$ km s^{-1}, where $k_{\rm B} = 1.38 \times 10^{-16}$ erg K^{-1} is the Boltzmann constant and $m_{\rm g} = 3.34 \times 10^{-24}$ g is the gas molecule mass, which value corresponds to H_2 gas.

2.3. *Chondrule dynamics*

The velocity of chondrules with respect to the shock front, v, will change as follows (e.g., Hood & Horanyi 1991):

$$\frac{4\pi}{3}r^3\rho\frac{{\rm d}v}{{\rm d}x} = -\frac{C_{\rm D}}{2}\pi r^2\rho_{\rm g}\frac{|v - v_{\rm g}|}{v}(v - v_{\rm g}), \quad (4)$$

where $C_{\rm D}$ is the drag coefficient, r is the chondrule radius, and $\rho = 3.3$ g cm^{-3} is the internal density of chondrules (Ciesla et al. 2004). Assuming that the temperature of chondrules is equal to gas temperature, the drag coefficient, $C_{\rm D}$, is given by

$$C_{\rm D} = \frac{2\sqrt{\pi}}{3s} + \frac{2s^2 + 1}{\sqrt{\pi}s^3}\exp\left(-s^2\right) + \frac{4s^4 + 4s^2 - 1}{2s^4}{\rm erf}(s), \quad (5)$$

where the Mach number, s, is given by $s \equiv |v - v_{\rm g}|/c_{\rm s}$. Here we introduce the stopping length of chondrules, $l_{\rm stop}$. For the case in which chondrules move in gas with supersonic velocities, $l_{\rm stop}$ is approximately given by

$$l_{\rm stop} \equiv \left(\frac{1}{v}\left|\frac{{\rm d}v}{{\rm d}x}\right|\right)^{-1} \simeq \frac{4}{3}\frac{\rho}{\rho_{\rm g}}\left(\frac{v - v_{\rm g}}{v}\right)^{-2} r. \quad (6)$$

If the spatial scale of shock is much larger than the stopping length ($L \gg l_{\rm stop}$), the velocity of a chondrule reaches $v \simeq v_{\rm post}$ behind the shock front, while v barely changes when $L \ll l_{\rm stop}$ (see Arakawa & Nakamoto 2019). On the other hand, for the case in which chondrules move in gas with subsonic velocities, $l_{\rm stop}$ is approximately given by the following equation:

$$l_{\rm stop} \simeq 0.64\frac{\rho}{\rho_{\rm g}}\left(\frac{c_{\rm s}|v - v_{\rm g}|}{v^2}\right)^{-1} r. \quad (7)$$

2.4. *Accretion of fine-grained rims*

In this study, we calculate the accretion of fine-grained rim in shock waves. The mass accretion rate per unit length, ${\rm d}m/{\rm d}x$, is given by

$$\frac{{\rm d}m}{{\rm d}x} = Q\rho_{\rm d}\pi r^2\frac{v_{\rm imp}}{v}, \quad (8)$$

where Q is the coefficient for adhesion/erosion of fine grains, and $\rho_{\rm d}$ is the dust density. Here we assume that fine grains are both dynamically and thermally coupled with gas, and the impact velocity of fine grains is given by

$$v_{\rm imp} = |v - v_{\rm g}|. \quad (9)$$

The growth rate of the thickness of rims, ${\rm d}r/{\rm d}x$, is given by the following equation:

$$\frac{{\rm d}r}{{\rm d}x} = \frac{1}{4\pi\rho r^2}\frac{{\rm d}m}{{\rm d}x}, \quad (10)$$

and we do not consider the porosity of FGRs for simplicity.[1] The thickness of the rim, Δ, is given by

$$\Delta = r - r_0, \quad (11)$$

where r_0 is the radius of the bare chondrule.

The coefficient for adhesion/erosion depends on the impact velocity: $Q = Q(v_{\rm imp})$. In this study, we assume that $Q(v_{\rm imp})$ is given by a step function as follows:

$$Q = \begin{cases} Q_{\rm ad} & (v_{\rm min} \leq v_{\rm imp} \leq v_{\rm max}), \\ Q_{\rm er} & (v_{\rm imp} > v_{\rm max}\ {\rm and}\ \Delta > 0), \\ 0 & ({\rm otherwise}), \end{cases} \quad (12)$$

where $Q_{\rm ad}$ and $Q_{\rm er}$ are the coefficients for adhesion/erosion, and $v_{\rm max}$ and $v_{\rm min}$ are the maximum/minimum velocity for adhesion, respectively. We change the values of $Q_{\rm ad}$, $Q_{\rm er}$, $v_{\rm max}$, and $v_{\rm min}$ as parameters (see Table 1).

We do not consider the erosion of chondrules for simplicity; however, it might play an important role for the origin

[1] The porosity of FGRs formed via the kinetic dust aggregation process would be 10% or less (e.g., Hanft et al. 2015), although it must depend on many parameters including the impact velosity and the material composition.

Table 1. Fundamental parameters for describing the accretion of FGRs: $Q_{\rm ad}$, $Q_{\rm er}$, $v_{\rm max}$, and $v_{\rm min}$.

Parameter	Symbol	Value
Coefficient for adhesion	$Q_{\rm ad}$	0.5 or 0.2
Coefficient for erosion	$Q_{\rm er}$	0 or -1
Maximum velocity for adhesion	$v_{\rm max}$	1 km s^{-1} or 0.3 km s^{-1}
Minimum velocity for adhesion	$v_{\rm min}$	0.1 km s^{-1} or 0.3 km s^{-1}

of a non-zero constant in the linear relationship between Δ and r_0 reported from observations of chondrules in CM chondrites (Liffman 2019). The erosion of chondrules may also be problematic in the context of the survival of chondrules in shock waves if $Q_{\rm er} \ll -1$ (e.g., Jacquet & Thompson 2014). However, we can imagine that the value of $Q_{\rm er}$ for the erosion of chondrules should differ from that for the erosion of FGRs, and our knowledge of erosion of chondrules is still limited. Thus, future studies on the physics of erosive collision are necessary.

2.5. *Production of silicate dust from evaporating planetesimals*

We simply set the following assumption for the structure of $\rho_{\rm d}$:

$$\rho_{\rm d} = \begin{cases} 0 & (x < 0), \\ \chi \rho_{\rm g} & (x \geq 0), \end{cases} \tag{13}$$

where χ is the dust-to-gas mass ratio in the dusty region formed behind the shock front. In this study, we set $\chi = 1$ based on the order-of-magnitude analysis shown below.

In this study, we consider the evaporation of undifferentiated icy planetesimals. The planetesimal surface is heated by a hot shocked gas, and the surface ice evaporates. For the case of the supersonic limit, Tanaka et al. (2013) derived that the evaporation flux of the surface ice of the planetesimal is approximately given by

$$J_{\rm ice} \simeq \pi {R_{\rm p}}^2 \frac{2\gamma}{(\gamma+1)^2} \frac{\alpha \rho_{\rm g,0} {v_0}^3}{L_{\rm eva}}, \tag{14}$$

where $L_{\rm eva} = 2.7 \times 10^{10}$ erg g^{-1} is the latent heat of evaporation of ice, and α is the non-dimensional parameter called the Stanton number, which expresses the efficiency of heat conduction. Tanaka et al. (2013) found that the realistic range of α for planetesimal bow shocks is $10^{-2} \leq \alpha \leq 10^{-1}$. When the surface ice evaporates, dust grains are also released from the surface of undifferentiated planetesimals. The mass flux of the released dust grains, $J_{\rm dust}$, would be simply given as follows:

$$J_{\rm dust} = f_{\rm dust/ice} J_{\rm ice}, \tag{15}$$

where $f_{\rm dust/ice}$ is the dust-to-ice mass ratio of the evaporating undifferentiated planetesimals.

The value of $f_{\rm dust/ice}$ is uncertain; however, several studies on the internal structure of comet 67P/Churyumov–Gerasimenko suggested that the dust-to-ice mass ratio of the comet is significantly higher than one, $f_{\rm dust/ice} \gg 1$ (e.g., Fulle et al. 2019; Pätzold et al. 2019; Arakawa & Ohno 2020). The bulk density of the comet indicates $f_{\rm dust/ice} \simeq 9$ (Arakawa & Ohno 2020) if comets are formed via gravitational collapse of a cloud of dust aggregates in the solar nebula (e.g., Skorov & Blum 2012; Wahlberg Jansson & Johansen 2017; Visser et al. 2021). Fulle et al. (2019) also reviewed the dust-to-ice mass ratio of other comet nuclei visited by space missions and of trans-Neptunian objects (TNOs), and these objects have generally the value of $f_{\rm dust/ice} \gg 3$.

These estimates on the value of $f_{\rm dust/ice}$ are an order of magnitude higher than the classical value for the dust composition in protoplanetary disks (e.g., Pollack et al. 1994; D'Alessio et al. 2001). We note, however, that recent studies on the dust composition of protoplanetary disks (see Birnstiel et al. 2018, and references therein) suggest that $f_{\rm dust/ice}$ should be several times higher than that predicted by Pollack et al. (1994). Tazaki et al. (2021) also evaluated the dust-to-ice mass ratio using the scattering polarization in the envelope of the low mass protostar L1551 IRS 5, and they found that icy dust grains with the radius of a few μm (or larger) and $f_{\rm dust/ice} \gtrsim 10$ are consistent with the observed polarization excess around a wavelength of 3 μm. Thus, we can expect that icy planetesimals are formed from dust-rich icy grains with $f_{\rm dust/ice} \gg 1$.

Assuming the mass conservation, the dust density is given by

$$\rho_{\rm d} \simeq \frac{J_{\rm dust}}{\pi {R_{\rm d}}^2 v_{\rm g}}, \tag{16}$$

where $R_{\rm d}$ is the radius of the dusty region. Then, the typical value of the dust-to-gas mass ratio behind the shock front would be obtained as follows:

$$\begin{aligned} \chi &\simeq f_{\rm dust/ice} \left(\frac{R_{\rm p}}{R_{\rm d}}\right)^2 \frac{2\gamma}{(\gamma+1)^2} \frac{\alpha {v_0}^2}{L_{\rm eva}} \\ &\simeq 0.8 \left(\frac{f_{\rm dust/ice}}{9}\right) \left(\frac{R_{\rm d}/R_{\rm p}}{3}\right)^{-2} \left(\frac{\alpha}{0.03}\right) \left(\frac{v_0}{12\ {\rm km\ s^{-1}}}\right)^2. \end{aligned} \tag{17}$$

Therefore, the value of $\chi \simeq 1$ could be achieved in the dusty region caused by the evaporation of undifferentiated icy planetesimals, although there are large uncertainties of the values of $f_{\rm dust/ice}$, $R_{\rm p}/R_{\rm d}$, and α. Thus, future studies on the detailed analysis on the dust-to-gas mass ratio behind the shock front would be essential.

The diameter-density relation among TNOs are investigated so far (e.g., Brown 2012; Grundy et al. 2019). Large TNOs whose diameter is larger than 1000 km have usually the bulk density of approximately 2–3 g cm^{-3}, while mid-sized TNOs with a diameter smaller than 1000 km have the bulk density of approximately 1 g cm^{-3}. Grundy et al.

(2019) pointed out that difference in bulk density may reflect the porosity change. Thus, icy planetesimals with a diameter smaller than 1000 km would be porous and undifferentiated bodies, and the dusty region may be formed when shock waves are caused by these mid-sized planetesimals. In contrast, large icy bodies with a diameter larger than 1000 km would be differentiated and might not be suitable for the formation of rimmed chondrules.

3. RESULTS

3.1. *Impact velocity*

First, we show the impact velocity of fine grains. Figure 3 shows $v_{\rm imp}$ as a function of the distance from the shock front. Panels (a), (b), and (c) show the results for the cases of $L = 3 \times 10^4$ km, $L = 1 \times 10^4$ km, and $L = 3 \times 10^3$ km, respectively. Solid lines indicate $v - v_{\rm g} < 0$ while dashed line indicate $v - v_{\rm g} > 0$.

Arakawa & Nakamoto (2019) found that the dynamical evolution of chondrules in shock waves can be divided into two stages: deceleration region behind the shock front (Stage 1) and recovery region where the velocity of chondrules and gas approach the pre-shock velocity (Stage 2). As shown in Figure 3, the change of Stages 1/2 occurred at around $x \sim 1000$ km for the case of $\rho_{\rm g,0} = 5 \times 10^{-10}$ g cm^{-3}, and small chondrules enter Stage 2 earlier than larger chondrules. This is because smaller chondrules have shorter stopping lengths (see Equations 6 and 7). For the cases of $L \geq 1 \times 10^4$ km, $v_{\rm imp}$ in Stage 2 is approximately proportional to the radius of the bare chondrule r_0. In Discussion section, we will derive $v_{\rm imp} = v_{\rm imp}(r_0)$ in Stage 2 from an analytical argument.

3.2. *Evolution of rim thickness*

Then, we show the evolution of the thickness of FGRs in the dusty region. We introduce the results for two cases: rim formation without erosion ($Q_{\rm er} = 0$) and with erosion ($Q_{\rm er} = -1$).

3.2.1. *Rim formation without erosion*

Figure 4 shows the thickness of FGRs, Δ, as a function of x and r_0. Panels (a), (b), and (c) show the results for the cases of $L = 3 \times 10^4$ km, $L = 1 \times 10^4$ km, and $L = 3 \times 10^3$ km, respectively. Here we set $Q_{\rm ad} = 0.5$, $Q_{\rm er} = 0$, $v_{\rm max} = 1$ km s^{-1}, and $v_{\rm min} = 0.1$ km s^{-1}.

As shown in Figure 4, FGRs with thickness of 10–100 μm are formed via the kinetic dust aggregation process. We found that the thickness of FGRs formed in Stage 1 is significantly smaller than the final thickness in these simulations; therefore the FGRs are mainly formed in Stage 2. In addition, for the case of large $L = 3 \times 10^4$ km, the thickness is approximately proportional to r_0. We derived analytical solutions for the rim thickness formed in Stages 1 and 2 in Discussion section, and the analytical solutions reproduce the linear relationship between Δ and r_0.

3.2.2. *Rim formation with erosion*

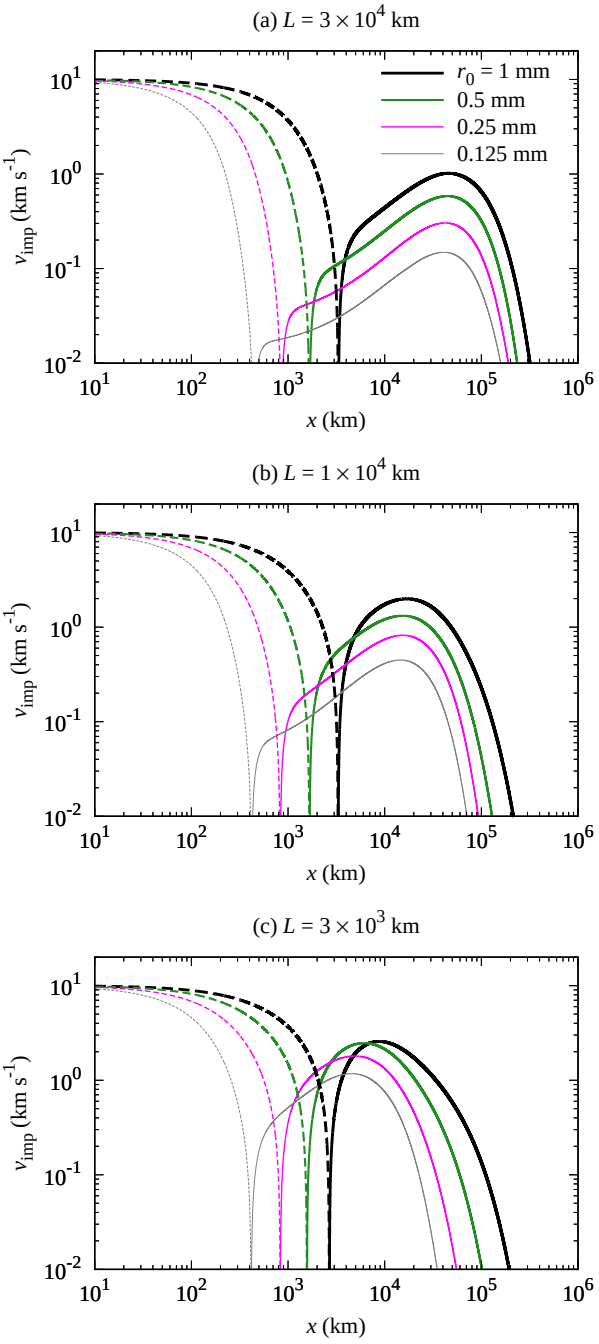


Figure 3. Impact velocity of fine grains, $v_{\rm imp} = |v - v_{\rm g}|$. (a) For the case of $L = 3 \times 10^4$ km. (b) For the case of $L = 1 \times 10^4$ km. (c) For the case of $L = 3 \times 10^3$ km. Solid lines indicate $v - v_{\rm g} < 0$ while dashed lines indicate $v - v_{\rm g} > 0$. We set $Q_{\rm ad} = 0.5$, $Q_{\rm er} = 0$, $v_{\rm max} = 1$ km s^{-1}, and $v_{\rm min} = 0.1$ km s^{-1}.

However, in reality, FGRs would be eroded when $v_{\rm imp}$ is higher than the critical value for erosion. Although the exact value of the coefficient for erosion, $Q_{\rm er}$, is highly uncertain, the assumption of $Q_{\rm er} < 0$ seems to be more realistic than $Q_{\rm er} = 0$. Figure 5 shows the thickness of FGRs, Δ, as a

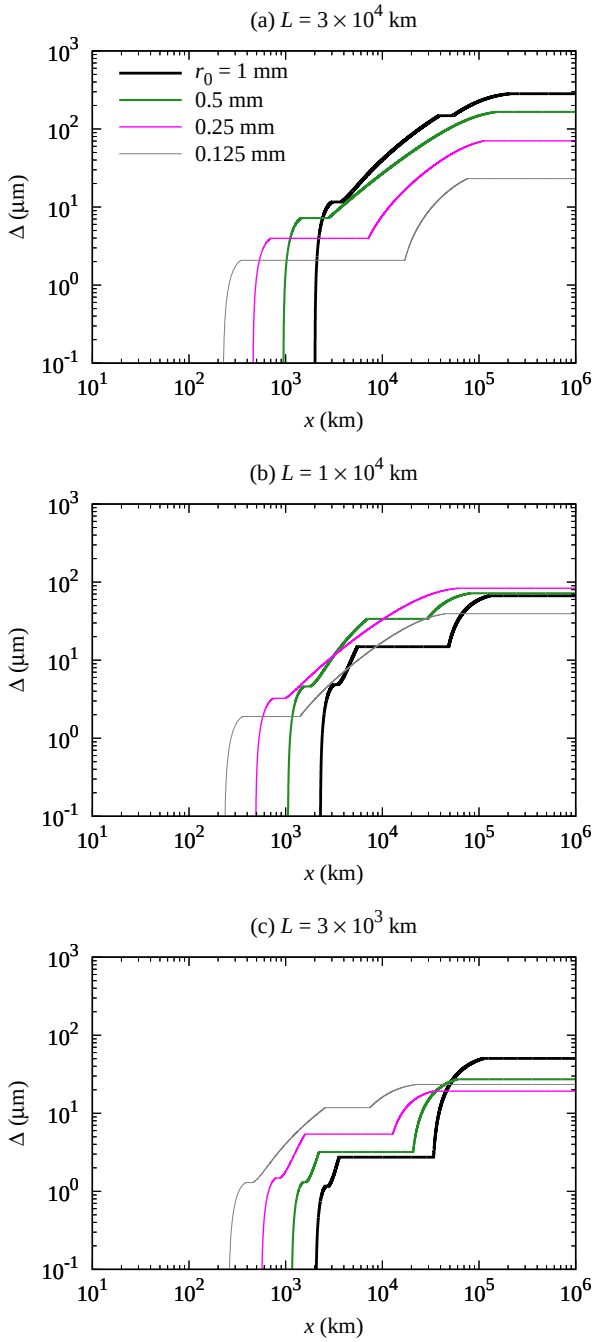


Figure 4. Thickness of fine-grained rims, $\Delta - r - r_0$. (a) For the case of $L = 3 \times 10^4$ km. (b) For the case of $L = 1 \times 10^4$ km. (c) For the case of $L = 3 \times 10^3$ km. We set $Q_{\rm ad} = 0.5$, $Q_{\rm er} = 0$, $v_{\rm max} = 1$ km s^{-1}, and $v_{\rm min} = 0.1$ km s^{-1}, and rim formation without erosion is assumed.

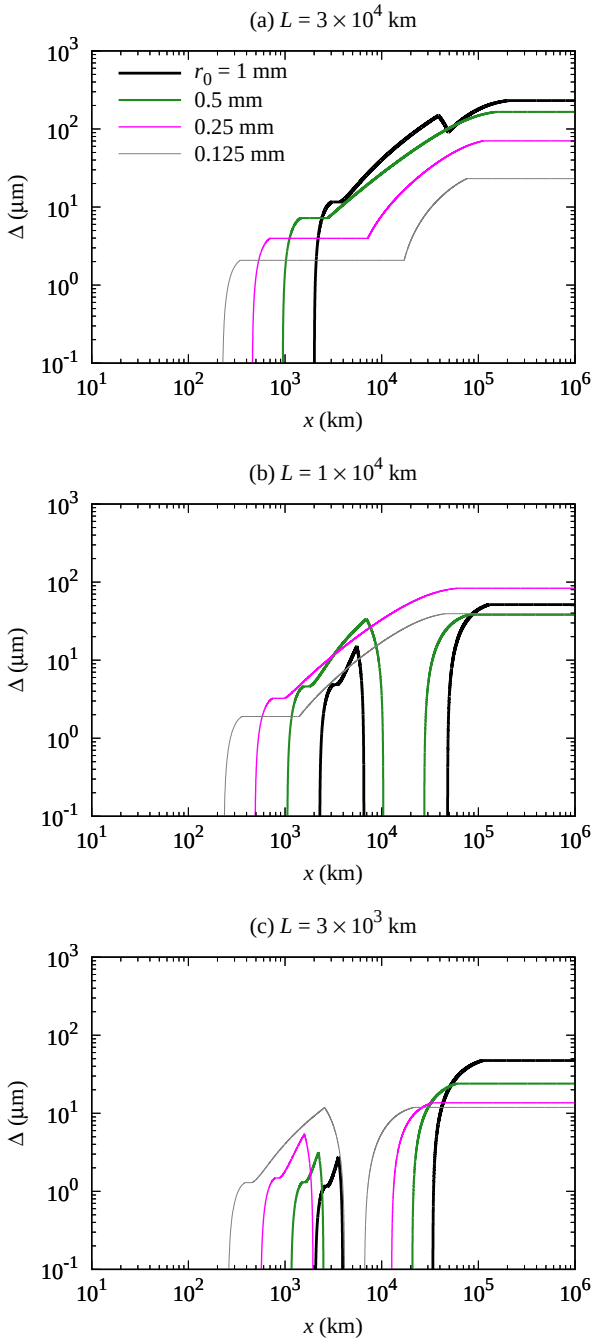


Figure 5. Thickness of fine-grained rims, $\Delta - r - r_0$. (a) For the case of $L = 3 \times 10^4$ km. (b) For the case of $L = 1 \times 10^4$ km. (c) For the case of $L = 3 \times 10^3$ km. We set $Q_{\rm ad} = 0.5$, $Q_{\rm er} = -1$, $v_{\rm max} = 1$ km s^{-1}, and $v_{\rm min} = 0.1$ km s^{-1}, and rim formation with erosion is assumed.

function of x and r_0. Panels (a), (b), and (c) show the results for the cases of $L = 3 \times 10^4$ km, $L = 1 \times 10^4$ km, and $L = 3 \times 10^3$ km, respectively. We set $Q_{\rm ad} = 0.5$, $Q_{\rm er} = -1$, $v_{\rm max} = 1$ km s^{-1}, and $v_{\rm min} = 0.1$ km s^{-1}.

Figure 5(a) shows the evolution of Δ for the case of $L = 3 \times 10^4$ km. For the case of $r_0 = 1$ mm (black line), the erosion of FGRs occurs at around $x \simeq 5 \times 10^4$ km but FGRs partly survive after erosion. Then fine dust grains accrete onto chondrules again; multi-layered FGRs would be formed

by single shock-heating event. Interestingly, many chondrules in Kivesvaara CM2 chondrite are covered by multi-layered FGRs (Metzler et al. 1992) and our scenario might explain the origin of these multi-layered FGRs. Our scenario also indicates that inner rims formed in a hotter environment than outer rims. This would be consistent with the observed characteristics of inner rims (e.g., silicate sintering, sulfides growth, and compaction; Zanetta et al. 2021).

Figure 5(b) shows the evolution of Δ for the case of $L = 1 \times 10^4$ km. For the cases of $r_0 = 1$ mm (black line) and $r_0 = 0.5$ mm (green line), FGRs formed before erosion are completely eroded once, then re-accretion of FGRs occurs. Similar evolutionary path are also found in Figure 5(c), i.e., for the case of $L = 3 \times 10^3$ km. We note that the final thickness of FGRs is in the range of 10–100 μm even if we take into account the effect of erosion. This is because the final thickness of FGRs is mainly controlled by the accretion of fine grains in Stage 2.

3.3. *Dependence of final rim thickness on chondrule radius*

Finally, we show the dependence of final rim thickness on chondrule radius. Figure 6 shows the results for the case of $Q_{\rm er} = 0$ (rim formation without erosion) and Figure 7 is for the case of $Q_{\rm er} = -1$ (rim formation with erosion). As shown in Figures 4 and 5, FGR formation finishes at $x \sim 10^5$ km because $v_{\rm imp} < v_{\rm min}$ for $x \gg 10^5$ km. Then we stop numerical simulations at $x = 10^6$ km in this study.

Figure 6(a) shows the results for the case of $Q_{\rm ad} = 0.5$, $Q_{\rm er} = 0$, $v_{\rm max} = 1$ km s^{-1}, and $v_{\rm min} = 0.1$ km s^{-1}. We found that the final rim thickness is approximately consistent with that for chondrules in Murchison CM chondrite: $(\Delta/1\ \mu{\rm m}) = 0.11(r_0/1\ \mu{\rm m}) + 24.5$ (Hanna & Ketcham 2018). The value of Δ also depends on the spatial scale of the shock, L, and our numerical results show a good agreement with observations for CM chondrites when $L = 1 \times 10^4$ km or 3×10^4 km.

Figure 6(b) shows the results for the case of $Q_{\rm ad} = 0.2$, $Q_{\rm er} = 0$, $v_{\rm max} = 1$ km s^{-1}, and $v_{\rm min} = 0.1$ km s^{-1}. As the accretion rate of FGRs is proportional to $Q_{\rm ad}$, the final thickness of FGRs formed in this setting is smaller than that shown in Figure 6(a). We found that the final rim thickness is in the range of 5 μm $\leq \Delta \leq$ 40 μm for the cases of $L = 1 \times 10^4$ km and 3×10^3 km. This is consistent with the thickness of FGRs around chondrules in unequilibrated ordinary chondrites (Matsunami 1984). The observations by Matsunami (1984) indicate that the thickness of FGRs is not dependent on the chondrule radius, and similar results are also reported by Bigolski (2017).

We note that our results are based on simple one-dimensional simulations. However, in reality, shock waves caused by eccentric planetesimals are bow shocks. The trajectories of chondrules are curved and strongly depend on their size (e.g., Boley et al. 2013; Katsuda 2017). Moreover, we assumed that the coefficient for adhesion is constant in the range of $v_{\rm min} < v_{\rm imp} < v_{\rm max}$; this assumption also seems to be unlikely. For these reasons, we do not discuss the detailed features of the dependence of Δ on r_0 in this study.

Figure 6(c) shows the results for the case of $Q_{\rm ad} = 0.5$, $Q_{\rm er} = 0$, $v_{\rm max} = 1$ km s^{-1}, and $v_{\rm min} = 0.3$ km s^{-1}. Interestingly, the thickness of FGRs is significantly smaller than the observed values when $L = 3 \times 10^4$ km and $r_0 < 300$ μm. This is because the maximum value of $v_{\rm imp}$ in Stage 2 is lower than 0.3 km s^{-1} if the radius of chondrules is smaller than 300 μm, as shown in Figure 3(a). In this case, FGRs cannot be formed in Stage 2 and final thickness would be equal to the thickness formed in Stage 1.

Figure 6(d) shows the results for the case of $Q_{\rm ad} = 0.5$, $Q_{\rm er} = 0$, $v_{\rm max} = 0.3$ km s^{-1}, and $v_{\rm min} = 0.1$ km s^{-1}. Although the final thickness of FGRs is smaller than that formed in Figure 6(a), FGRs with thickness of 10–100 μm are formed even if $v_{\rm max} = 0.3$ km s^{-1}. In conclusion, the kinetic dust aggregation in shock waves around evaporating icy planetesimals would be the leading candidate for the origin of FGRs around chondrules in primitive chondrites.

Figure 7 shows the results for the case of FGR formation with erosion ($Q_{\rm er} = -1$). Although the final thickness of FGRs formed in Figure 7 is slightly smaller than that in Figure 6 ($Q_{\rm er} = 0$), the general trends are similar and FGRs with thickness of 10–100 μm are formed even if we consider the effect of erosion. This is consistent with the fact that the thickness of FGRs formed in Stage 1 is significantly smaller than that formed in Stage 2.

The relation between the thickness of FGRs and the radius of chondrules is discussed so far. For chondrules in carbonaceous chondrites, the positive correlation was reported within the range of 100 μm $< r_0 <$ 1000 μm (e.g., Hanna & Ketcham 2018). In contrast, no clear correlation between Δ and r_0 was found for chondrules in unequilibrated ordinary chondrites (Matsunami 1984). Our results show that the positive correlation appears when accretion of FGRs occurs in the almost all region of Stage 2 (see Figure 4(a)).

4. DISCUSSION

4.1. *Rim thickness formed in Stage 1: deceleration region behind the shock front*

As mentioned above, the thickness of FGRs formed in Stage 1 is significantly smaller than that formed in Stage 2. Here we derive an analytic solution for the thickness of FGRs formed in Stage 1. The motion of chondrules in Stage 1 is described as the deceleration behind the shock front.

Here we consider the accretion of fine dust grains onto chondrules in Stage 1, and we assume that $v_{\rm g}$, $\rho_{\rm g}$, and $c_{\rm s}$ are almost constant for simplicity. Although the relative velocity of chondrules with respect to gas is supersonic at $x \ll l_{\rm stop}$, FGRs are not formed in this region because $v_{\rm imp}$ is higher than the maximum velocity for adhesion, $v_{\rm max}$. Then $v_{\rm imp}$ will drop to the range for adhesion, and FGR formation in Stage 1 will start.

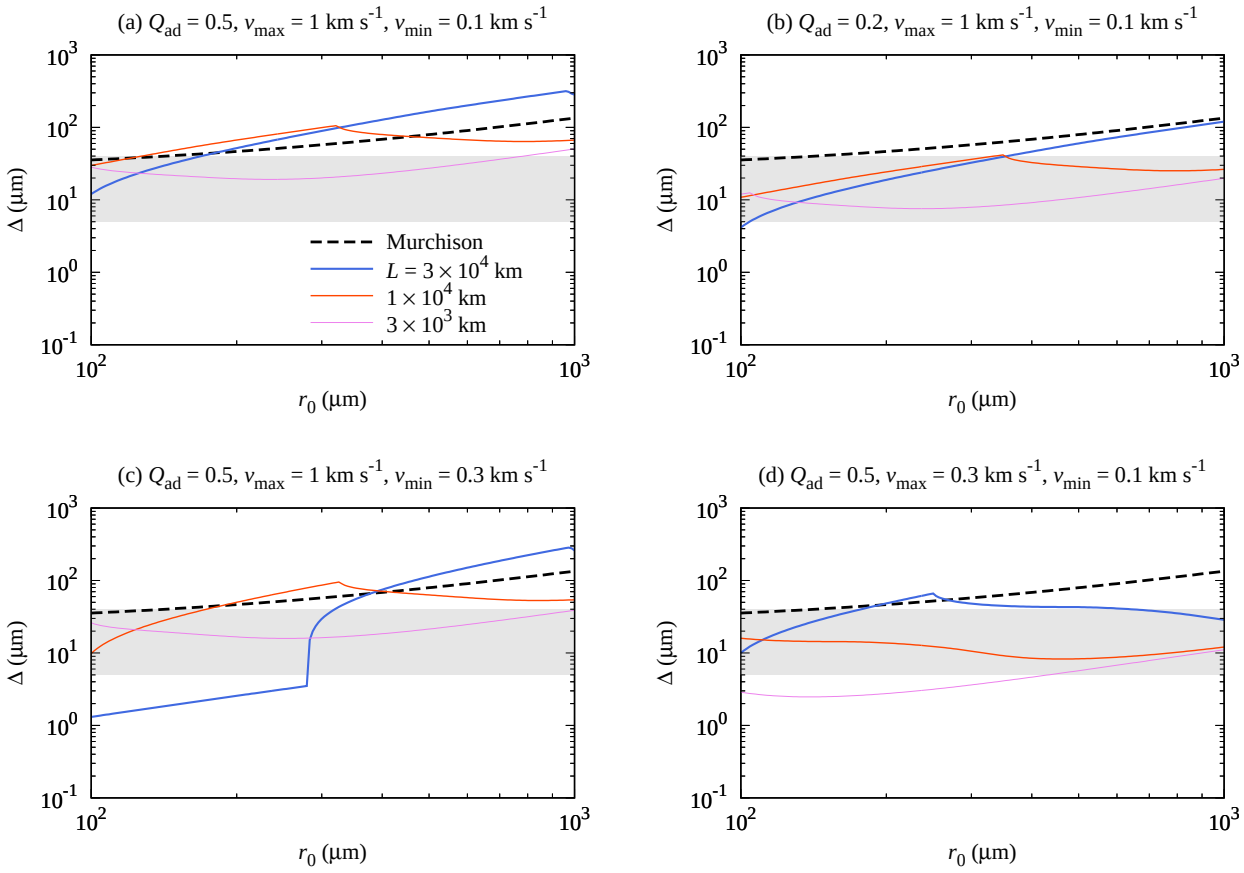


Figure 6. Thickness of FGRs, Δ, as a function of chondrule radius, r_0. Fine-grained rim formation without erosion is assumed: $Q_{\rm er} = 0$. The black dashed line indicates the relationship between Δ and r_0 for chondrules in Murchison CM chondrite: $(\Delta/1\ \mu{\rm m}) = 0.11(r_0/1\ \mu{\rm m}) + 24.5$ (Hanna & Ketcham 2018). The gray shaded range indicates the typical thickness of FGRs around chondrules in unequilibrated ordinary chondrites: $5\ \mu{\rm m} \leq \Delta \leq 40\ \mu{\rm m}$ (Matsunami 1984).

When the relative velocity of chondrules with respect to gas is subsonic, the time evolution of $v_{\rm imp}$ is given by

$$\frac{{\rm d}v_{\rm imp}}{{\rm d}t} \simeq -\left|\frac{{\rm d}v}{{\rm d}t}\right| \simeq -\frac{1}{0.64}\frac{\rho_{\rm g}}{\rho}\frac{c_{\rm s}v_{\rm imp}}{r_0}. \quad (18)$$

For the case of $v_{\rm min} < v_{\rm imp} < v_{\rm max}$, the time evolution of the radius of rimmed chondrules is given by

$$\frac{{\rm d}r}{{\rm d}t} = \frac{Q_{\rm ad}}{4}\frac{\rho_{\rm d}}{\rho}v_{\rm imp} \simeq -\frac{0.64Q_{\rm ad}}{4}\chi\frac{r_0}{c_{\rm s}}\frac{{\rm d}v_{\rm imp}}{{\rm d}t}. \quad (19)$$

Then the thickness of FGRs formed in Stage 1 would be approximately given by the following equation:

$$\Delta_1 = \frac{0.64Q_{\rm ad}}{4}\chi\frac{v_{\rm max}-v_{\rm min}}{c_{\rm s}}r_0 \simeq 2\left(\frac{Q_{\rm ad}}{0.5}\right)\left(\frac{\chi}{1}\right)\left(\frac{v_{\rm max}-v_{\rm min}}{900\ {\rm m\ s^{-1}}}\right)\left(\frac{r_0}{100\ \mu{\rm m}}\right)\ \mu{\rm m}. \quad (20)$$

Our analytic solution suggests that the thickness of FGRs formed in stage 1 is $\Delta_1 \simeq 2\ (r_0/100\,\mu{\rm m})\ \mu{\rm m}$, and this value is one order of magnitude smaller than the observed thickness of FGRs around chondrules in CM chondrites (e.g., Hanna & Ketcham 2018). Thus we need to consider the FGR formation in Stage 2.

4.2. *Rim thickness formed in Stage 2: quasi-steady state in recovery region*

Similarly, we can derive the analytic solution for the thickness of FGRs formed in Stage 2. When the spatial scale of the shock is sufficiently larger than the stopping length ($L \gg l_{\rm stop}$), the motion of chondrules in Stage 2 is described as the dynamically quasi-steady state. In this region, the velocities of both gas and chondrules recover (see Equation 1), and the relative velocity of the chondrule to the gas is negligibly smaller than $v_{\rm g}$ (see also Arakawa & Nakamoto 2019).

When we consider the quasi-steady state for the dynamics of chondrules in Stage 2, the differential of the velocity of chondrules is approximately given by the following equa-

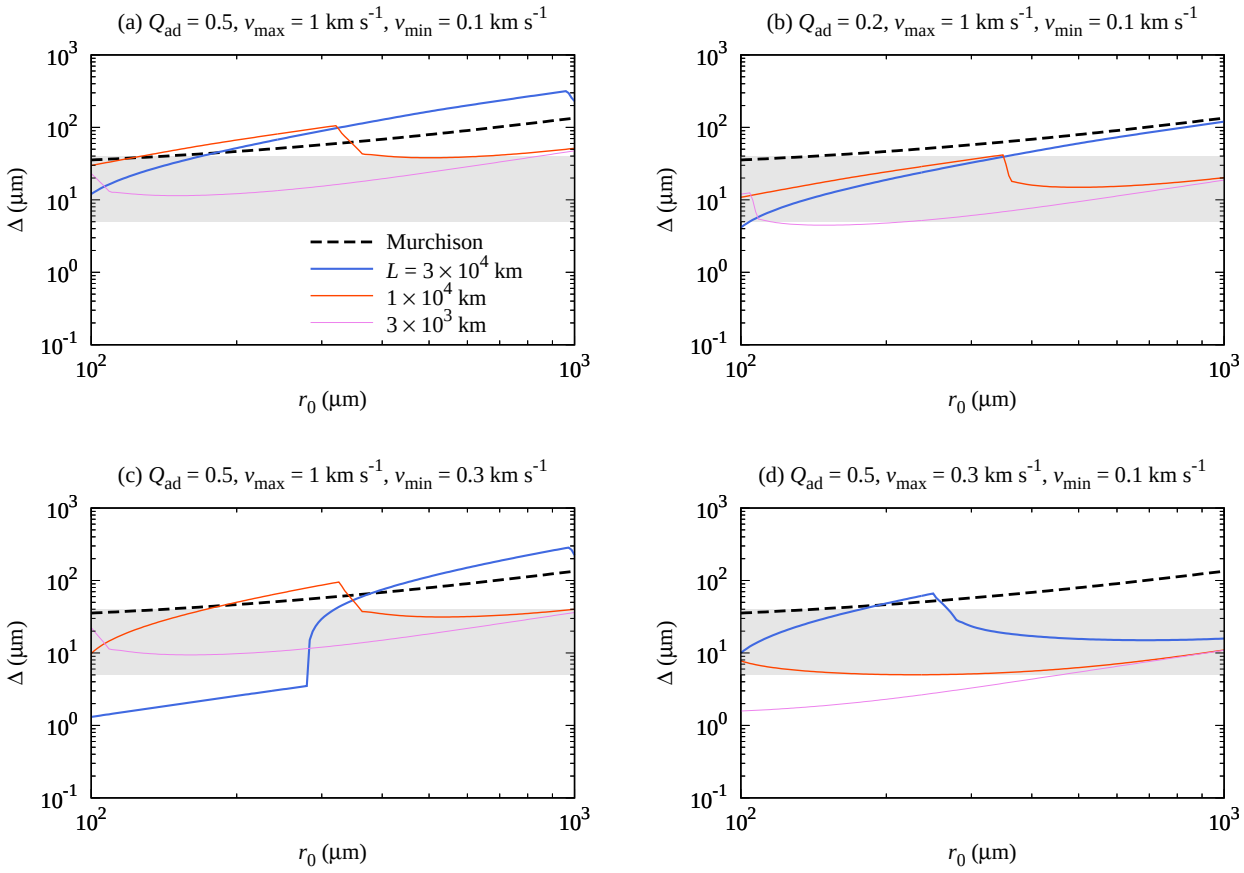


Figure 7. Thickness of FGRs, Δ, as a function of chondrule radius, r_0. Fine-grained rim formation with erosion is assumed: $Q_{\rm er} = -1$. The black dashed line indicates the relationship between Δ and r_0 for chondrules in Murchison CM chondrite: $(\Delta/1\ \mu{\rm m}) = 0.11(r_0/1\ \mu{\rm m}) + 24.5$ (Hanna & Ketcham 2018). The gray shaded range indicates the typical thickness of FGRs around chondrules in unequilibrated ordinary chondrites: $5\ \mu{\rm m} \leq \Delta \leq 40\ \mu{\rm m}$ (Matsunami 1984).

tion:

$$\left|\frac{{\rm d}v}{{\rm d}x}\right| = \frac{v}{l_{\rm stop}} \simeq \frac{v_{\rm g}}{l_{\rm stop}} \simeq \frac{1}{0.64}\frac{\rho_{\rm g}}{\rho}\frac{c_{\rm s}}{v_{\rm g}}\frac{v_{\rm imp}}{r_0}. \quad (21)$$

On the other hand, the differential of the velocity of gas is given as follows (see Equation 1):

$$\left|\frac{{\rm d}v_{\rm g}}{{\rm d}x}\right| = \frac{|v_{\rm g} - v_0|}{L}. \quad (22)$$

Assuming that ${\rm d}v/{\rm d}x$ and ${\rm d}v_{\rm g}/{\rm d}x$ are approximately equal, the relative velocity of the chondrule from the gas, which is equal to $v_{\rm imp}$, is derived as follows:

$$v_{\rm imp} \simeq 0.64\frac{\rho}{\rho_{\rm g}}\frac{v_{\rm g}}{c_{\rm s}}\frac{|v_{\rm g} - v_0|}{L}r_0. \quad (23)$$

As $v_{\rm imp}$ takes the maximum at around $x \sim L$, we show the value of $v_{\rm imp}$ at $x = L$ as a reference:

$$v_{\rm imp}|_{x=L} \simeq 120\left(\frac{\rho_{\rm g,0}}{5\times10^{-10}\ {\rm g\ cm^{-3}}}\right)^{-1} \times\left(\frac{L}{3\times10^4\ {\rm km}}\right)^{-1}\left(\frac{r_0}{100\ \mu{\rm m}}\right){\rm m\ s^{-1}}. \quad (24)$$

Then we can calculate the time evolution of the radius of rimmed chondrules. When the impact velocity of fine dust grains satisfies $v_{\rm min} < v_{\rm imp} < v_{\rm max}$, the differential of the radius of rimmed chondrules is given by

$$\frac{{\rm d}r}{{\rm d}x} = \frac{Q_{\rm ad}}{4}\frac{\rho_{\rm d}}{\rho}\frac{v_{\rm imp}}{v} \simeq \frac{0.64Q_{\rm ad}}{4}\chi\frac{|v_{\rm g} - v_0|}{c_{\rm s}}\frac{r_0}{L}. \quad (25)$$

The maximum thickness formed in Stage 2, $\Delta_{2,\rm max}$, is therefore given by the following equation:

$$\Delta_{2,\rm max} = \int_0^\infty {\rm d}x\,\frac{{\rm d}r}{{\rm d}x} \simeq 32\left(\frac{Q_{\rm ad}}{0.5}\right)\left(\frac{\chi}{1}\right)\left(\frac{r_0}{100\ \mu{\rm m}}\right)\mu{\rm m}. \quad (26)$$

We found that $\Delta_{2,\max} \gg \Delta_1$, thus FGRs would be mainly formed in Stage 2, quasi-steady state in recovery region. The maximum thickness of FGRs formed in stage 2 is $\Delta_{2,\max} \simeq 32\ (r_0/100\ \mu\mathrm{m})\ \mu\mathrm{m}$, and this value can explain the existence of thick FGRs around chondrules found in CM chondrites (e.g., Hanna & Ketcham 2018).

We note that the thickness of FGRs formed in Stage 2 is approximately equal to $\Delta_{2,\max}$ only when $v_{\min} < v_{\mathrm{imp}}|_{x=L} < v_{\max}$. When $v_{\mathrm{imp}}|_{x=L} \gg v_{\max}$, the thickness of FGRs is smaller than $\Delta_{2,\max}$ because fine dust grains cannot accrete onto chondrules at around $x \sim L$. This effect appears in the blue line in Figures 6(d) and 7(d); FGRs around chondrules with radius larger than $0.25\ \mathrm{mm}$ are thinner than $\Delta_{2,\max}$. In addition, FGRs are not formed in Stage 2 when $v_{\mathrm{imp}}|_{x=L} \ll v_{\min}$.

We also note that the power-law exponent for the relation between Δ and r_0 (for chondrules in carbonaceous chondrites) is still under debate. Although several studies (e.g., Metzler et al. 1992; Cuzzi 2004) reported that Δ is approximately proportional to r_0, Hanna & Ketcham (2018) pointed out that Δ is approximately proportional to the square root of r_0. When accretion of FGRs occurs in the entire region of Stage 2, our model predicts that Δ is proportional to ${r_0}^{1-\beta}$, where β is the exponent for the velocity dependence of Q_{ad} (i.e., Q_{ad} is proportional to ${v_{\mathrm{imp}}}^{-\beta}$). Thus the relation between Δ and r_0 could be reproduced if $\beta \simeq 0.5$ in the range of $v_{\min} < v_{\mathrm{imp}} < v_{\max}$. Although we set $\beta = 0$ (i.e., Q_{ad} is constant) in this preliminary study, we need to investigate the velocity dependence of Q_{ad} from laboratory experiments.

4.3. *Co-existence of rimmed and unrimmed chondrules*

Although FGRs are frequently observed around chondrules in primitive chondrites, the occurrence rate is not 100%. For unequilibrated ordinary chondrites, the occurrence rate is 79% for Semarkona, 70% for Watonga, and 59% for Bishunpur (Bigolski & Weisberg 2017). In addition, the occurrence rate of FGRs is only 15–20% for Allende CV chondrite (Simon et al. 2018). Therefore, we must give an explanation for the co-existence of rimmed and unrimmed chondrules in the context of FGR formation. Several mechanisms were proposed so far: Tomeoka & Ohnishi (2010) claimed that unrimmed chondrules have lost FGRs during the brecciation process on their parent bodies, whereas Umstätter & Urbassek (2021) proposed that unrimmed chondrules were formed via collisional fragmentation of chondritic aggregates in the solar nebula.

In our scenario, FGRs are formed via the kinetic dust aggregation process in the dusty region formed behind the evaporating icy planetesimal. We note that dusty regions would be formed only when shock waves are caused by undifferentiated icy planetesimals; no dusty regions are expected for the case of differentiated planetesimals. Therefore, if chondrules are formed via shock-wave heating events caused by both undifferentiated and differentiated planetesimals, we can expect the co-existence of rimmed and unrimmed chondrules. As the critical diameter of icy planetesimals for differentiation would be approximately 1000 km, parts of chondrules might be formed via shock waves caused by huge planetesimals (or protoplanets) whose diameter is far larger than 1000 km.

4.4. *The oxygen isotope ratios and Mg# systematics of chondrules*

The Mg# of chondrules, which is defined as Mg# = [MgO] / [MgO + FeO] in molar percent, reflects the oxidation state of iron during chondrule formation, and we can estimate the environment of chondrule formation (e.g., oxygen fugacity) from the Mg#. The mass-independent oxygen isotope fractionation, Δ^{17}O, is also useful to estimate the redox conditions and dust-to-ice mass ratio in chondrule formation environment (e.g., Tenner et al. 2015; Hertwig et al. 2018; Williams et al. 2020). Tenner et al. (2015) calculated the dust-to-gas and dust-to-ice mass ratios in chondrule formation environment for chondrules in CR chondrites. Using the mass balance and the equilibrium condensation model, they reported that type I (Mg# > 90) chondrules would be formed in moderately dust-rich environments (100–200 times the solar metallicity) and from ice-dust mixtures with 0–0.8 times the abundance of ice in CI chondrites. Similar results are also reported by Hertwig et al. (2018) for type I chondrules in CV chondrites.

When chondrules formed via bow shocks around evaporating undifferentiated icy planetesimals, Equation (17) predicted that the degree of dust enrichment would be on the order of 100 (i.e., the dust-to-gas mass ratio is on the order of 1). This value is approximately consistent with the results from Mg#–Δ^{17}O systematics for type I chondrules in carbonaceous chondrites (e.g., Williams et al. 2020). The dust-to-ice mass ratio in chondrule formation environment would be approximately equal to the bulk composition of the planetesimals. Therefore, undifferentiated icy planetesimals with slightly dust-rich compared to the CI composition might be suitable to reproduce the oxygen isotope ratios and Mg# systematics. We will discuss the redox conditions and dust-to-ice mass ratio in chondrule formation environment in future studies.

5. SUMMARY

FGRs are frequently found around chondrules in primitive chondrites. The remarkable feature of FGRs is their submicron-sized and non-porous nature (e.g., Trigo-Rodriguez et al. 2006; Chizmadia & Brearley 2008). The typical thickness of FGRs around chondrules is 10–100 μm.

Liffman (2019) proposed an idea for the origin of FGRs: high-speed collisions between chondrules and fine dust grains, which is called the kinetic dust aggregation process (see Hanft et al. 2015, and references therein). The resulting dust layer formed via the kinetic dust aggregation would have low porosity and be fine grained. Therefore, it would be possible to reproduce the observed structure of FGRs if they are formed via the kinetic dust aggregation process, which should be related to chondrule-forming supersonic events.

In this study, we examined the possibility of FGR formation via kinetic dust aggregation in chondrule-forming shock

waves (see Figure 2). When shock waves are caused by undifferentiated icy planetesimals, fine dust grains would be released from the planetary surface due to evaporation of icy planetesimals (e.g., Tanaka et al. 2013). Then the dusty region would be formed behind the shock front. We studied the dynamics of chondrules behind the shock front using simple one-dimensional calculations, and the growth of FGRs via kinetic dust aggregation was investigated. Our key findings are summarized as follows.

1. As Arakawa & Nakamoto (2019) pointed out, the dynamical evolution of chondrules in shock waves can be divided into two stages: deceleration region behind the shock front (Stage 1) and recovery region where the velocity of chondrules and gas approach the pre-shock velocity (Stage 2). We showed that $v_{\rm imp}$ is approximately proportional to r_0 in Stage 2.

2. We found that non-porous FGRs with the thickness of 10–100 μm are formed in shock waves around evaporating icy planetesimals (Figures 4 and 5). This thickness is in good agreement with observations (e.g., Matsunami 1984; Hanna & Ketcham 2018). We also found that the thickness of FGRs formed in Stage 1 is significantly smaller than that formed in Stage 2.

3. We derived analytic solutions for the thickness of FGRs formed in Stages 1 and 2. The motion of chondrules in Stage 1 is described as the deceleration behind the shock front, while the motion of chondrules in Stage 2 is described as the dynamically quasi-steady state. Our analytical solutions also predict that the thickness of FGRs is proportional to the chondrule radius when the effect of erosion is negligible.

4. In some cases, the erosion of FGRs occurs but FGRs partly survive after erosion, and fine dust grains accrete onto chondrules again (see Figure 5). Thus multi-layered FGRs would be formed by single shock-heating event; this might be consistent with the fact that chondrules in some CM2 chondrites are covered by multi-layered FGRs (Metzler et al. 1992).

5. Although FGRs are frequently observed around chondrules in primitive chondrites, the occurrence rate is not 100%. In our scenario, FGR formation would proceed in the dusty region formed behind the evaporating icy planetesimal. We note that dusty regions would be formed only when shock waves are caused by undifferentiated icy planetesimals; no dusty regions are expected for the case of differentiated planetesimals. Therefore, if chondrules are formed via shock-wave heating events caused by both undifferentiated and differentiated planetesimals, we can expect the coexistence of rimmed and unrimmed chondrules.

ACKNOWLEDGMENTS

The anonymous reviewer provided a constructive review that improved this paper. The authors thank Yuji Matsumoto for helpful comments. S.A. was supported by JSPS KAKENHI Grant No. JP20J00598. T.N. was supported by JSPS KAKENHI Grant No. JP18K03721.

REFERENCES

Akedo, J. 2006, Journal of the American Ceramic Society, 89, 1834

—. 2008, Journal of Thermal Spray Technology, 17, 181

Akedo, J., Nakano, S., Park, J., Baba, S., & Ashida, K. 2008, Synthesiology English edition, 1, 121

Alexander, C. M. O. D., Grossman, J. N., Ebel, D. S., & Ciesla, F. J. 2008, Science, 320, 1617, doi: 10.1126/science.1156561

Arakawa, S. 2017, The Astrophysical Journal, 846, 118, doi: 10.3847/1538-4357/aa8564

Arakawa, S., & Nakamoto, T. 2019, The Astrophysical Journal, 877, 84, doi: 10.3847/1538-4357/ab1b3e

Arakawa, S., & Ohno, K. 2020, Monthly Notices of the Royal Astronomical Society, 497, 1166, doi: 10.1093/mnras/staa2031

Beitz, E., Blum, J., Mathieu, R., Pack, A., & Hezel, D. C. 2013a, Geochimica et Cosmochimica Acta, 116, 41, doi: 10.1016/j.gca.2012.04.059

Beitz, E., Güttler, C., Nakamura, A. M., Tsuchiyama, A., & Blum, J. 2013b, Icarus, 225, 558, doi: 10.1016/j.icarus.2013.04.028

Bigolski, J. N. 2017, The Formation of Fine-Grained Chondrule Rims in Unequilibrated Ordinary Chondrites (City University of New York (Ph.D. thesis))

Bigolski, J. N., & Weisberg, M. K. 2017, in 80th Annual Meeting of the Meteoritical Society, Vol. 80, 6234

Birnstiel, T., Dullemond, C. P., Zhu, Z., et al. 2018, The Astrophysical Journal Letters, 869, L45, doi: 10.3847/2041-8213/aaf743

Bland, P. A., Howard, L. E., Prior, D. J., et al. 2011, Nature Geoscience, 4, 244, doi: 10.1038/ngeo1120

Boley, A. C., Morris, M. A., & Desch, S. J. 2013, The Astrophysical Journal, 776, 101, doi: 10.1088/0004-637X/776/2/101

Brown, M. E. 2012, Annual Review of Earth and Planetary Sciences, 40, 467, doi: 10.1146/annurev-earth-042711-105352

Chizmadia, L. J., & Brearley, A. J. 2008, Geochimica et Cosmochimica Acta, 72, 602, doi: 10.1016/j.gca.2007.10.019

Ciesla, F. J., Hood, L. L., & Weidenschilling, S. J. 2004, Meteoritics & Planetary Science, 39, 1809, doi: 10.1111/j.1945-5100.2004.tb00077.x

Cuzzi, J. N. 2004, Icarus, 168, 484, doi: 10.1016/j.icarus.2003.12.008

D'Alessio, P., Calvet, N., & Hartmann, L. 2001, The Astrophysical Journal, 553, 321, doi: 10.1086/320655

Daneshian, B., & Assadi, H. 2014, Journal of Thermal Spray Technology, 23, 541, doi: 10.1007/s11666-013-0019-4

Fulle, M., Blum, J., Green, S. F., et al. 2019, Monthly Notices of the Royal Astronomical Society, 482, 3326, doi: 10.1093/mnras/sty2926

Grundy, W. M., Noll, K. S., Buie, M. W., et al. 2019, Icarus, 334, 30, doi: 10.1016/j.icarus.2018.12.037

Hanft, D., Exner, J., Schubert, M., et al. 2015, Journal of Ceramic Science and Technology, 6, 147

Hanna, R. D., & Ketcham, R. A. 2018, Earth and Planetary Science Letters, 481, 201, doi: 10.1016/j.epsl.2017.10.029

Hertwig, A. T., Defouilloy, C., & Kita, N. T. 2018, Geochimica et Cosmochimica Acta, 224, 116, doi: 10.1016/j.gca.2017.12.013

Hewins, R. H., Zanda, B., & Bendersky, C. 2012, Geochimica et Cosmochimica Acta, 78, 1, doi: 10.1016/j.gca.2011.11.027

Hood, L. L., & Horanyi, M. 1991, Icarus, 93, 259, doi: 10.1016/0019-1035(91)90211-B

Jacquet, E., & Thompson, C. 2014, The Astrophysical Journal, 797, 30, doi: 10.1088/0004-637X/797/1/30

Johnson, S. D., Glaser, E. R., Cheng, S.-F., Kub, F. J., & Eddy, Charles R., J. 2014, Applied Physics Express, 7, 035501, doi: 10.7567/APEX.7.035501

Kaneko, H., Arakawa, S., & Nakamoto, T. 2022, Icarus, 374, 114726, doi: 10.1016/j.icarus.2021.114726

Katsuda, Y. 2017, Planetesimal Bow Shocks with High Dust-to-Gas Mass Ratio: A Possible Chondrule Formation Site (Tokyo Institute of Technology (master thesis))

Lauretta, D. S., Hua, X., & Buseck, P. R. 2000, Geochimica et Cosmochimica Acta, 64, 3263, doi: 10.1016/S0016-7037(00)00425-7

Liffman, K. 2019, Geochimica et Cosmochimica Acta, 264, 118, doi: 10.1016/j.gca.2019.08.009

Mai, C., Desch, S. J., Boley, A. C., & Weiss, B. P. 2018, The Astrophysical Journal, 857, 96, doi: 10.3847/1538-4357/aab711

Mann, C. R., Boley, A. C., & Morris, M. A. 2016, The Astrophysical Journal, 818, 103, doi: 10.3847/0004-637X/818/2/103

Matsumoto, Y., Hasegawa, Y., Matsuda, N., & Liu, M.-C. 2021, Icarus, 367, 114538, doi: 10.1016/j.icarus.2021.114538

Matsumoto, Y., Wakita, S., Hasegawa, Y., & Oshino, S. 2019, The Astrophysical Journal, 887, 248, doi: 10.3847/1538-4357/ab5b06

Matsunami, S. 1984, National Institute Polar Research Memoirs, 35, 126

Metzler, K., Bischoff, A., & Stoeffler, D. 1992, Geochimica et Cosmochimica Acta, 56, 2873, doi: 10.1016/0016-7037(92)90365-P

Morfill, G. E., Durisen, R. H., & Turner, G. W. 1998, Icarus, 134, 180, doi: 10.1006/icar.1998.5948

Morris, M. A., Boley, A. C., Desch, S. J., & Athanassiadou, T. 2012, The Astrophysical Journal, 752, 27, doi: 10.1088/0004-637X/752/1/27

Nagasawa, M., Tanaka, K. K., Tanaka, H., et al. 2019, The Astrophysical Journal, 871, 110, doi: 10.3847/1538-4357/aaf795

Pätzold, M., Andert, T. P., Hahn, M., et al. 2019, Monthly Notices of the Royal Astronomical Society, 483, 2337, doi: 10.1093/mnras/sty3171

Pollack, J. B., Hollenbach, D., Beckwith, S., et al. 1994, The Astrophysical Journal, 421, 615, doi: 10.1086/173677

Schrader, D. L., Connolly, H. C., Lauretta, D. S., et al. 2013, Geochimica et Cosmochimica Acta, 101, 302, doi: 10.1016/j.gca.2012.09.045

Sears, D. W. G., Benoit, P. H., & Jie, L. 1993, Meteoritics, 28, 669, doi: 10.1111/j.1945-5100.1993.tb00638.x

Simon, J. I., Cuzzi, J. N., McCain, K. A., et al. 2018, Earth and Planetary Science Letters, 494, 69, doi: 10.1016/j.epsl.2018.04.021

Skorov, Y., & Blum, J. 2012, Icarus, 221, 1, doi: 10.1016/j.icarus.2012.01.012

Takayama, A., & Tomeoka, K. 2012, Geochimica et Cosmochimica Acta, 98, 1, doi: 10.1016/j.gca.2012.08.015

Tanaka, K. K., Yamamoto, T., Tanaka, H., et al. 2013, The Astrophysical Journal, 764, 120, doi: 10.1088/0004-637X/764/2/120

Tazaki, R., Murakawa, K., Muto, T., Honda, M., & Inoue, A. K. 2021, The Astrophysical Journal, 910, 26, doi: 10.3847/1538-4357/abdd3d

Tenner, T. J., Nakashima, D., Ushikubo, T., Kita, N. T., & Weisberg, M. K. 2015, Geochimica et Cosmochimica Acta, 148, 228, doi: 10.1016/j.gca.2014.09.025

Tomeoka, K., & Ohnishi, I. 2010, Geochimica et Cosmochimica Acta, 74, 4438, doi: 10.1016/j.gca.2010.04.058

Trigo-Rodriguez, J. M., Rubin, A. E., & Wasson, J. T. 2006, Geochimica et Cosmochimica Acta, 70, 1271, doi: 10.1016/j.gca.2005.11.009

Umstätter, P., & Urbassek, H. M. 2021, Astronomy & Astrophysics, 652, A40, doi: 10.1051/0004-6361/202141581

Visser, R. G., Drążkowska, J., & Dominik, C. 2021, Astronomy & Astrophysics, 647, A126, doi: 10.1051/0004-6361/202039769

Wahlberg Jansson, K., & Johansen, A. 2017, Monthly Notices of the Royal Astronomical Society, 469, S149, doi: 10.1093/mnras/stx1470

Weidenschilling, S. J., Marzari, F., & Hood, L. L. 1998, Science, 279, 681, doi: 10.1126/science.279.5351.681

Williams, C. D., Sanborn, M. E., Defouilloy, C., et al. 2020, Proceedings of the National Academy of Science, 117, 23426, doi: 10.1073/pnas.2005235117

Xiang, C., Carballido, A., Hanna, R. D., Matthews, L. S., & Hyde, T. W. 2019, Icarus, 321, 99, doi: 10.1016/j.icarus.2018.10.014

Xiang, C., Carballido, A., Matthews, L. S., & Hyde, T. W. 2021, Icarus, 354, 114053, doi: 10.1016/j.icarus.2020.114053

Zanetta, P. M., Leroux, H., Le Guillou, C., Zanda, B., & Hewins, R. H. 2021, Geochimica et Cosmochimica Acta, 295, 135, doi: 10.1016/j.gca.2020.12.015